Robust Brain MRI Denoising and Segmentation Using Enhanced non-local Means Algorithm

Muhammad Aksam Iftikhar, Abdul Jalil, Saima Rathore, Mutawarra Hussain

Department of Computer and Information Sciences, Pakistan Institute of Engineering and Applied Sciences, Islamabad, Pakistan

Received 20 July 2013; accepted 7 November 2013

ABSTRACT: Image denoising is an integral component of many practical medical systems. Non-local means (NLM) is an effective method for image denoising which exploits the inherent structural redundancy present in images. Improved adaptive non-local means (IANLM) is an improved variant of classical NLM based on a robust threshold criterion. In this paper, we have proposed an enhanced non-local means (ENLM) algorithm, for application to brain MRI, by introducing several extensions to the IANLM algorithm. First, a Rician bias correction method is applied for adapting the IANLM algorithm to Rician noise in MR images. Second, a selective median filtering procedure based on fuzzy c-means algorithm is proposed as a postprocessing step, in order to further improve the quality of IANLM-filtered image. Third, different parameters of the proposed ENLM algorithm are optimized for application to brain MR images. Different variants of the proposed algorithm have been presented in order to investigate the influence of the proposed modifications. The proposed variants have been validated on both T1-weighted (T1-w) and T2-weighted (T2-w) simulated and real brain MRI. Compared with other denoising methods, superior quantitative and qualitative denoising results have been obtained for the proposed algorithm. Additionally, the proposed algorithm has been applied to T2-weighted brain MRI with multiple sclerosis lesion to show its superior capability of preserving pathologically significant information. Finally, impact of the proposed algorithm has been tested on segmentation of brain MRI. Quantitative and qualitative segmentation results verify that the proposed algorithm based segmentation is better compared with segmentation produced by other contemporary techniques. Int J Imaging Syst Technol, 24, 52–66, 2014; Published online in Wiley Online Library (wileyonlinelibrary.com). DOI: 10.1002/ima.22079

Key words: non-local means; denoising; brain MRI; segmentation; Rician noise

I. INTRODUCTION

Brain MR Image analysis is a common clinical activity which is used to diagnose many neurological diseases such as Alzheimer's disease, multiple sclerosis, brain tumor, etc. A computer-aided system helps automating this clinical activity in order to obtain faster and reliable analysis. However, the intrinsic noise present in brain MR images severly limits the performance of such computer-aided systems. The sources of noise in brain MR images include movement of patient, limitations of imaging equipment, human error etc. The noise should be removed in brain MRI prior to any subsequent processing in order to obtain adequate performance.

The traditional approaches to digital image denoising include wavelet filtering (Donoho, 1995; Selesnick, 2004; Luisier et al., 2007), total variation minimization (Osher et al., 2005), diffusion filtering (Perona and Malik, 1990; Gilboa et al., 2004) and local neighborhood based filtering (Tomasi and Manduchi, 1998). A relatively recent approach to image denoising is weighted averaging of pixels based on patch comparison. Buades et al. (2005) proposed a non-local means (NLM) filter following this approach which has proven to be successful in many denoising applications. It not only removes noise from the input image in an effective manner but also preserves image details. The main idea is to exploit the natural redundancy in the input image to restore better quality image. In particular, a pixel is restored by computing weighted mean of pixels within a search window around it (ideally the whole image). The weights are computed by comparing the local neighborhood of each pixel (called its patch) with neighborhoods of pixels in the search window. This approach is similar to Yaroslavsky work, however, it involves comparison of patches rather than comparison of pixels as in (Yaroslavsky, 1985). Due to the intrinsic self-redundancy in images, the comparison of patches is expected to be reliable and robust to noise compared with simple pixels' based comparison.

The original NLM algorithm compares patches within whole image which is computationally intractable. Limiting the search area to a particular search window improves computational efficiency of the algorithm without much deterioration of denoising performance. Aksam et al. proposed a search window adaptation mechanism for the conventional NLM algorithm based on a robust threshold criterion (Aksam et al., 2013). Their proposed algorithm, called improved adaptive non-local means (IANLM), is not only computationally faster than traditional NLM but also yields better denoising results. Thaipanich and Kuo (2010) also proposed an adaptive search window algorithm based on different region types. Salmon (2010) presented yet another study related to the search window size and central patch weight which is another improtant

Correspondence to: Iftikhar Muhammad Aksam; e-mail: aksam.iftikhar@gmail.com

Grant sponsor: This research work is supported by PIEAS-administered Endowment Fund, provided by Higher Education Commission Pakistan, for higher education and R&D in IT and Telecom Sectors

parameter of the NLM algorithm. They concluded their study by suggesting suitable size of search window for each image used in their work. Yan et al. (2012) proposed a pixel pre-classification process prior to weight computation in NLM algorithm. The pre-classification process identified reliable set of candidate pixels for weighted aeraging in order to restore a particular pixel. Moreover, the authors employed rotationally invariant block matching (Grewenig et al., 2011) to improve the process of patch comparison. The work proposed in (Liu et al., 2008) presents an efficient and robust NLM variant by merging classical NLM with the Laplacian pyramid model.

In recent times, different variants of classical NLM have been proposed for application to brain MRI denoising. Manjon et al. proposed a variant, called unbiased non-local means (UNLM), wherein Rician bias correction is applied to the NLM algorithm to better deal with Rician noise in MRI data (Manjon et al., 2008). Yet another variant of NLM was proposed by Manjon et al., which uses wavelet mixing with classical NLM in order to take account of spatially varying noise in MRI data (Manjon et al., 2010). Vega et al. showed improved denoising and computational performance on brain MR images, by proposing salient features matching approach into the NLM framework (Vega et al., 2012). Their approach is based on comparison of key features of patches, rather than comparison of their intensity values only. Aksam et al. proposed a novel variant of genetic algorithm and used it to optimize parameters involved in classical NLM algorithm for application to brain MR images (Aksam et al., 2012).

The main contribution of this work is to propose a robust denoising method for restoring brain MR images corrupted with Rician noise. To be more precise, an enhanced non-local means (ENLM) algorithm has been presented by extending our previous work (Aksam et al., 2013) in several ways. First, ENLM offers special treatment of Rician noise (Gudbjartsson and Patz, 1995, Macovski, 1996), which is usually found in MR images. Second, an effective post processing operation, called selective median filtering (SMF), is proposed, which improves the restoration in homogeneous regions of the image. Finally, ENLM is characterized by optimization of several crucial parameters of the algorithm, for application to brain MR images. We have validated the performance of the proposed ENLM algorithm and its two variants on T1-w and T2-w simulated brain MR images with known noise levels. Quite promising quantitative and qualitative results have been obtained even at higher noise levels. The proposed ENLM algorithm has also been shown useful on real T1-w and T2-w brain MR images. Finally, the impact of the proposed ENLM algorithm has been studied on segmentation of brain MR images which is usually a successive stage after denoising. The non-local information in ENLM-filtered brain images has been incorporated into a fuzzy segmentation process and the segmentation results have been compared with a few segmentation techniques proposed in contemporary literature. Superior quantitative and qualitative results have been obtained which verify the positive effect of ENLM on the segmentation process.

The description of work in rest of this article is organized as follows. Section II describes various components of the proposed scheme in detail. Section III describes experimental setup for various experiments performed in this work. Section IV and V present the experiments conducted on simulated and real brain MRI, respectively. In Section VI, the impact of the proposed ENLM algorithm is investigated on segmentation of simulated brain MRI. Finally, the work is concluded in Section VII.

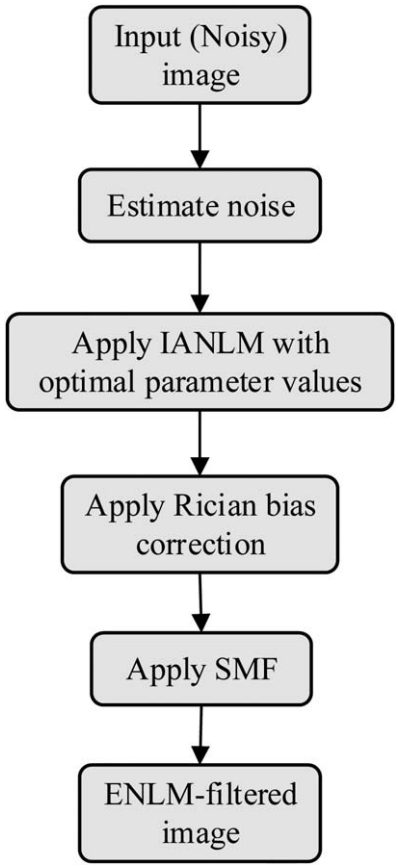

Figure 1. The proposed ENLM algorithm.

II. PROPOSED ENHANCED NON-LOCAL MEANS (ENLM) ALGORITHM

The proposed ENLM algorithm comprises various components, which have been described in detail in the following text. These components are listed as follows:

1. Estimation of noise (Section II (A)).
2. IANLM filtering (Section II (B)).
3. Adaptation to Ricain noise (Section II (C)).
4. Selective median filtering (SMF) (Section II (D)).
5. Optimization of parameters (Section II (E)).

These components should be applied (in the given sequence) to an input image in order to obtain the ENLM-filtered image. Figure 1 shows this process graphically. It is noteworthy that the optimization of parameters is required only once for a particular type of application (brain MRI in our case).

A. Estimation of Noise. Clinical MRI data usually contains Rician noise due to limitations of imaging equipment. However, the amount of noise is generally unknown. Therefore, some noise estimation method should be employed in order to assess the amount of noise in the input image. Several methods have been proposed in literature for estimation of Ricain noise in MR images. However, we have estimated the noise from squared magnitude MR images. This simple method for estimating the standard deviation $(\hat{\sigma})$ of Rician noise can be expressed mathematically as follows.

$$\hat{\sigma} = \sqrt{\frac{1}{2N}\sum_{k=1}^{N} M_k^2} \tag{1}$$

where, M represents the background part of the squared magnitude image. M_k denotes kth pixel of the background part, and N is total number of pixels in M. Note that $\hat{\sigma}$ is computed globally using Eq. (1), as the noise considered in this work is spatially uniform (constant).

B. Improved Adaptive Non-local Means (IANLM) algorithm. As already stated in Section I, we have extended the IANLM algorithm (an improved variant of classical NLM) in several ways. Therefore, we briefly describe the NLM and IANLM algorithms in this section. The NLM algorithm is based on computation of similarity weights between patches of noisy pixels within a search window. In the following text, the size (radius) of the search window and patch are denoted by s and p, respectively. The NLM-restored value of a particular pixel is computed as weighted sum of pixel values within the search window. Mathematically, the restoration process in NLM is expressed as follows:

$$x_i = \sum_{j \in S_i} w_{ij} y_j, \qquad \text{subject to} \quad \sum_{j \in S_i} w_{ij} = 1 \tag{2}$$

where y_j represents the jth pixel in the set of pixels (S_i) within the search window of pixel i, and x_i represents the NLM-restored value of pixel i. The similarity weight (w_{ij}) between patches $\boldsymbol{P_i}$ (patch of pixel i is referred to $\boldsymbol{P_i}$ in the following text) and $\boldsymbol{P_j}$ is computed using the following expression:

$$w_{ij} = \frac{1}{Z_i} e^{-\frac{\left(\|y(P_i) - y(P_j)\|_2^2\right)}{h^2}} \tag{3}$$

where h is the smoothing factor which controls the tradeoff between smoothness (noise removal) and detail preservation. $\|\boldsymbol{y(P_i)}\text{-}\boldsymbol{y(P_j)}\|_2$ denotes the Euclidian distance between patches $\boldsymbol{P_i}$ and $\boldsymbol{P_j}$, where $\boldsymbol{y(P_i)}$ and $\boldsymbol{y(P_j)}$ are the intensity values of pixels in Patch $\boldsymbol{P_i}$ and $\boldsymbol{P_j}$, respectively. The term Z_i is a normalization constant which makes sure that $w_{ij} \in [0, 1]$.

The IANLM algorithm introduces a search window adaptation mechanism into the basic NLM algorithm. The size of search window is selected adaptively based on a robust threshold criterion. The robust threshold criterion dictates that only a subset of pixels (*fit* pixels) within a search window participate in the restoration process. For each pixel, the search window size is determined adaptively based on number of fit pixels found within the search window for that pixel. The pixel restoration process in IANLM is expressed mathematically as follows.

$$x_i' = \sum_{j \in N_i^*} w_{ij} y_j, \qquad \text{subject to} \quad \sum_{j \in N_i^*} w_{ij} = 1 \tag{4}$$

where x_i' is the IANLM-restored value for pixel i and $N_i^* \subseteq S_i$ is the set of pixels around pixel i, satisfying following constraints.

- Robust threshold criterion: $w_{ij} > w_\theta$, where w_θ is the threshold on similarity between pixels i and j.
- Window adaptation test: $|N_i^*| \leq N_f$, where N_f designates fit pixels' cardinality within the search window.

C. Adaptation to Rician Noise. The noise in MR images follows Rician distribution which is known to be signal dependent. Due to different behavior of noise in low and high intensity regions, the overall contrast of an image is reduced. To eliminate such bias of Rician noise for different regions, it was proposed to filter the square of magnitude MR image rather than the image itself (Nowak, 1999). The effect of Rician noise can then be negated by subtracting the bias value from the restored value of each pixel (Wiest-Daesslé et al., 2008). The bias value usually equals double the variance of noise. Hence, the effect of bias can be negated by subtracting $2\sigma^2$ from the restored value, where σ is the standard deviation of noise in the image.

We have applied the said bias correction method to adapt IANLM to Rician noise. In particular, the squared magnitude MR images are restored by IANLM and unbiased value of each pixel is obtained by subtracting $2\sigma^2$ from its IANLM-restored value. This is expressed mathematically as follows.

$$x_i'' = \sqrt{x_i' - 2\sigma^2} \tag{5}$$

where x_i' represents the restored value of pixel i by IANLM algorithm, and x_i'' is unbiased restored value obtained after applying the bias correction.

D. Proposed Selective Median Filtering (SMF). The modifications proposed in IANLM restore better quality image from its noisy version. However, the window adaptation test in IANLM yields slightly deteriorated denoising for homogeneous regions at higher noise levels. This is shown for a brain MRI slice in Figure 3b where noisy pixels can still be seen in the zoomed portion of IANLM-filtered image. We conjecture that this irregularity induced by the IANLM algorithm can be fixed by applying median filtering to the restored image. However, simple median filtering strongly deteriorates the image quality near edges. Therefore, we have proposed a selective median filtering procedure based on Fuzzy C-Means segmentation, which is applied to the IANLM-filtered image as post processing.

Pseudo Code-I (The Selective Median Filtering process)

1. Input:
   a. $X' \leftarrow IANLM(Y)$, where Y is the noisy image.
   b. $N \leftarrow 4$, where N is number of segments in Y.
2. $Z \leftarrow fcm(X', N)$.
3. Set $i \leftarrow 1$.
4. For each segment S in Z
   REPEAT
      i. $S_b \leftarrow$ Boundary (S).
      ii. $M_i \leftarrow S - S_b$.
      iii. Set $i \leftarrow i+1$.
   END REPEAT
5. Compute $\varphi \leftarrow \sum_{i=1}^{N} M_i$ *(Obtain the mask image).*
6. $X'' \leftarrow Median(X', \varphi)$ *(Apply median filtering using mask* φ*).*
7. Output X''.

In the proposed selective median filtering process, the IANLM-restored image is segmented using FCM algorithm into four characteristic regions, namely white matter (WM), gray matter (GM), cerebrospinal fluid (CSF) and Background (BG). Median filtering (3×3) is then applied to the selected portion of each segment.

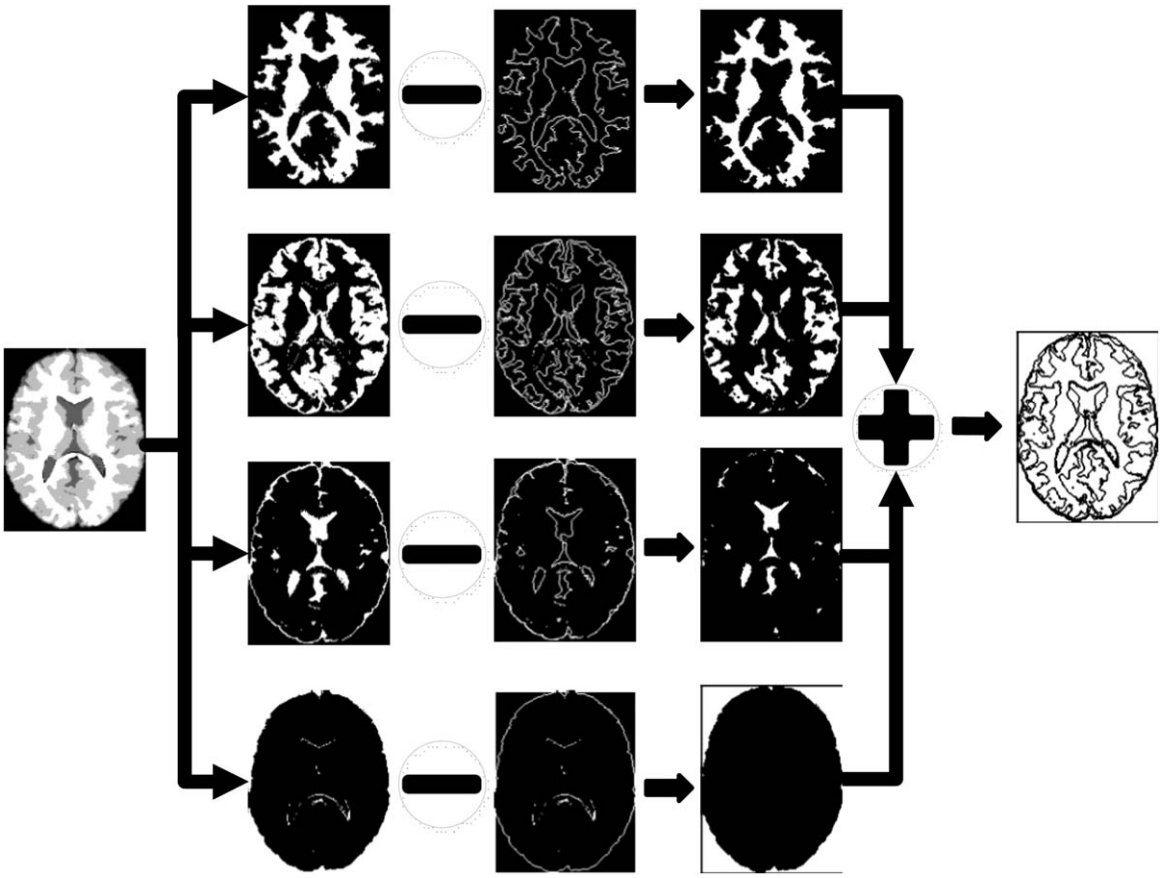

Figure 2. Obtaining mask for selective median filtering. 1st column: Image segmented by FCM corresponding to IANLM-filtered image in Figure 3b, 2nd column: Images corresponding to WM, GM, CSF and BG segments, 3rd column: Corresponding boundary pixels' images, 4th column: Corresponding individual mask images obtained after subtracting boundary images from original segment images, 5th column: Final mask image.

The selected portion corresponding to each segment is obtained by subtracting the boundary pixels from the original segment image**.** The selected portions are added to obtain an image which can be used as a single mask for median filtering. Thus, median filtering is applied only to the *on* pixels in the final mask image. A pseudo code for the proposed SMF process is presented in Pseudocode-I. The process of obtaining the final mask image for an IANLM-filtered image is also illustrated in Figure 2. The IANLM-filtered image and corresponding image obtained after applying SMF is shown in Figures 3b and 3c, respectively. By visual comparison of the zoomed portions in Figure 3, the improved quality of SMF-processed image can be observed easily.

E. Optimal Selection of Parameters. The IANLM algorithm involves a few parameters which should be tuned for a particular application in order to obtain optimized performance. In this work, we have optimized these parameters for application to brain MRI. A brief description of each of these parameters is given below.

A.1. Search Window Size (s). The IANLM algorithm is sensitive to this parameter, both in terms of denoising performance and computational efficiency. A very high value of this parameter typically results in better restoration quality, however, the cost incurred is added computational burden. On the other hand, a lower value is more feasible in terms of computational efficiency, but results in poor quality denoising. Therefore, a suitable tradeoff is required between denoising quality and computational efficiency.

B.1. Patch Size (p). The patch size designates the radius of the neighboring window around the pixel of interest. The denoising performance and computational efficiency of the algorithm depends on patch size (p, where $p < s$) which is an application dependent parameter. Therefore, a suitable value of this parameter is required for a particular application.

C.1. Scaling Factor (k). A suitable value of smoothing parameter is required in order to obtain a tradeoff between image smoothness and noise removal. A very high value may result in oversmoothing of the restored image. On the other hand, a very low value may yield undesirable artifacts in the restored image. For application to brain MRI, the smoothing parameter is directly related to the amount of noise in an image (Manjon et al., 2008), i.e. $h = k\sigma$, where k is a scaling factor and σ is the standard deviation of noise in the input image. The parameter σ can be estimated from the input image. Hence, it is the factor k which determines the suitable value of h for a particular application.

D.1. Central Pixel Weight (w'). The weight assigned to the central pixel is a special case of weight computation process. In case of central pixel, the two patches to be compared are identical. Therefore, according to Eq. (3), the weight corresponding to central pixel will always be equal to 1. This will bias the restored value of the pixel towards the original noisy pixel value. Therefore, a suitable

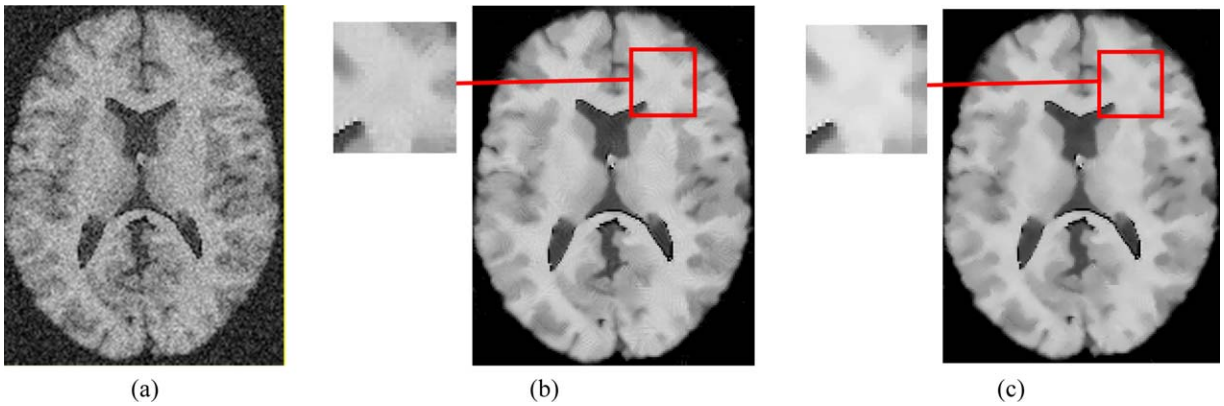

Figure 3. The effect of selective median filtering process, (a) A noisy brain image (Noise: 15%) (b) IANLM-filtered image (d) Image obtained after application of SMF, using mask in Figure 2, to (b). [Color figure can be viewed in the online issue, which is available at wileyonlinelibrary.com.]

weight assignment to the central pixel is necessary. For classical NLM, this parameter is simply set to the maximum weight value among weights of neighboring pixels. However, in order to obtain optimized performance, we have selected suitable value of this parameter for application to brain MRI.

E.1. Weight Threshold (w_0) and Desired Number of Fit Patches (N_f). These parameters are unique to IANLM and are not part of the original NLM algorithm. A higher value of N_f is desirable in order to obtain more robust denoising (see Section II (A)). On the other hand, increasing the value of N_f beyond a certain point merely adds to the computational burden. Therefore, a suitable value of N_f is desirable. Likewise, the value of w_θ is application dependent and should also be selected experimentally over a range of suitable values.

III. EXPERIMENTAL SETUP

In this work, following variants of the proposed ENLM algorithm have been considered for validation on brain MR data.

- ENLM (Enhanced NLM) adapts the IANLM filter to Rician noise and applies SMF as a post-processing step. Moreover, the values of different parameters are optimized for application to brain MRI.
- $ENLM_o$ (Optimization-void ENLM) is similar to ENLM, however, different parameters of the algorithm assume the values proposed in (Aksam et al., 2013), rather than the optimized values. This variant has been proposed to study the influence of optimization of parameters performed in this work.
- $ENLM_s$ (SMF-void ENLM) is similar to ENLM, however, it does not apply the selective median filtering procedure as post processing. This variant has been proposed to test the influence of the proposed selective median filtering process.

In this section, optimized values of different parameters (s, p, w', k, N_f, and w_θ) of ENLM algorithm are obtained for application to simulated brain MR data. In an optimization experiment for a particular parameter, values of all the parameters are fixed while only varying the parameter under investigation, within a suitable range of its values. Following *default* values (values of parameters, other than the parameter under investigation) have been used for various parameters: $S = 5$, $P = 2$, $w' = 0.1$, $k = 1$, $N_f = 60$ and $w_\theta = 0.01$. These values have been selected after substantial empirical testing. The optimal values of parameter, selected in this section, have been employed in different experiments performed in subsequent sections.

Two quantitative measures, namely Peak Signal to Noise Ratio (PSNR) and Structural Similarity Index Measure (SSIM) have been used to assess denoising performance. PSNR measures visual similarity between two images and is computed using the following expression.

$$\mathrm{PSNR} = 10\log_{10}(R^2/\mathrm{MSE}) = 20\log_{10}(R/\mathrm{RMSE}) \qquad (6)$$

where, R represents the maximum possible intensity value of a pixel in the image. For 8-bit gray level images, R is set to 255. RMSE is the root mean square error between the restored and original (ground truth) image. The other denoising performance measure, SSIM, was introduced to measure the similarity between structures of two images rather than the similarity between intensity values of their pixels (Wang et al., 2004). Valid range of values for this index vary from 0 (maximum deviation from ground truth) to 1 (identical to ground truth). SSIM between two images I and J can be computed using the following expression.

$$\mathrm{SSIM}(x,y) = \frac{(2\mu_I\mu_J + c_1)(2\sigma_{IJ} + c_2)}{(\mu_I^2 + \mu_J^2 + c_1)(\sigma_I^2 + \sigma_J^2 + c_2)} \qquad (7)$$

where in our case, I and J represent the reference and denoised images, respectively. μ_I and μ_J represent the mean intensity levels of I and J, and σ_I and σ_J are standard deviations of I and J, respectively. σ_{IJ} is the covariance of I and J; c_1 and c_2 are two constants depending on dynamic range of I and J.

Various experiments, performed in this work, have been conducted on a Core i7 system with 16 GB RAM and 3.4 GHz Turbo Boost CPU. MATLAB R2013a (8.1.0.604, http://www.mathworks.-com/products/matlab/) has been used as the computational tool (MATLAB 2013). OriginPro 9 (v9.0, http://www.originlab.com) has been used as a graphing tool (OriginPro 2012).

A. Data Set. In this work, both simulated and real brain MR images have been used in several experiments. The simulated brain MR images have been obtained from a database called BrainWeb (Collins et al., 1998). The images in the BrainWeb database have been generated by a MRI simulator (Kwan et al., 1996), and are available online. Both T1-w and T2-w simulated

brain volumes from the BrainWeb database have been used in our experiments. The slice thickness of 3D brain volumes is 1 mm and overall volume size is 181 × 217 × 181. Nonbrain tissues (skull, fat etc.) have been cropped with the help of a brain mask, which is constructed from segmentation ground truth available in the BrainWeb database. Thus, different experiments have been performed on the brain portion and average results, over all brain slices, have been reported.

The proposed algorithm has also been validated by performing experiments on real brain MRI. The real brain images have been obtained from the Open Access Series of Imaging Studies (OASIS), which is a publicly available clinical brain MRI database of various subjects (Marcus et al., 2007). We have performed denoising on structural MRI scans of different subjects in this database in order to assess the ability of proposed algorithm to remove the inherent noise in these images. A brain extraction algorithm from MIPAV (v7.0.1, http://mipav.cit.nih.gov/) (MIPAV 2013) has been used to extract brain portion from complete head MRI. A good reason for selecting the OASIS data set is that, both T1-w and T2-w MR scans are available for each subject. Therefore, denoising experiments have been performed on T1-w and T2-w real brain MRI and results have been shown for selected slices.

B. Selection of Parameters. As discussed earlier, the proposed algorithm involves a few critical parameters which need to be selected empirically in a particular application for optimized performance. In this section, we explore these values, over a potential range of values, for application to simulated brain MRI denoising. These values will be employed in different experiments performed in subsequent sections.

Figure 4 shows the performance of the proposed ENLM algorithm over suitable values of these parameters. Figures 4a and 4b show performance for search window size (s) and patch size (p). It can be observed from Figure 4a that, for lower noise levels, higher PSNR values are obtained with increase of s. However, for higher noise levels, no improvement is observed when s increases beyond a certain point. Therefore, a suitable tradeoff is obtained between the denoising performance and computational efficiency by selecting $s = 5$. Likewise, Figure 4b shows that for high noise levels, the PSNR values do not improve after $p = 2$. Rather, for low noise, the PSNR decreases for $p > 2$. Therefore, we select $p = 2$ for use in subsequent experiments.

Figures 4c and 4d demonstrate the performance of the proposed ENLM algorithm over suitable values of the scaling factor (k) and central pixel weight (w'). It is clear from Figure 4c that for all noise levels, peak performance is observed at $w' = 0.1$. A higher value of w' simply deteriorates the performance. Similarly, Figure 4d shows that a suitable tradeoff between PSNR values at lower and higher noise levels is obtained for $k = 1$.

Figures 4e and 4f present the performance for two important parameters of IANLM, namely number of fit patches (N_f) and weight threshold (w_θ). Figure 4e shows that higher PSNR values are obtained with the increase of N_f. However, little or no change in PSNR is observed after $N_f > 60$. It should be recognized that the higher the value of N_f, more will be the computational burden. Therefore, for optimized denoising and computational performance, $N_f = 60$ is the most viable option. Figure 4f shows that the PSNR values generally decrease with increase in value of w_θ. A suitable tradeoff between PSNR values at lower and higher noise levels is obtained for $w_\theta = 0.01$.

IV. EXPERIMETNS ON SIMULATED BRAIN MRI

In this section, we have performed several experiments for validation of the proposed ENLM algorithm on simulated T1-w and T2-w brain MRI. In Experiment I, the performance of the proposed ENLM algorithm has been compared with Unbiased NLM (UNLM)—an optimized variant of classical NLM algorithm adapted to Rician noise (see Section I). In Experiment II, the effect of parameter optimization and the proposed selective median filtering has been investigated on denoising performance of ENLM. In addition to UNLM in Experiment I, the proposed ENLM algorithm has also been compared with two other contemporary methods in Experiment III. Finally, in Experiment IV, the performance of the proposed ENLM algorithm is compared qualitatively with UNLM on a T2-weighted brain MRI with multiple sclerosis (MS) lesion. Table I summarizes the values of different parameters employed for different algorithms used in subsequent experiments. A hyphen symbol for a parameter value denotes that the parameter is not applicable to current algorithm. The values for Unbiased NLM have been inherited from (Manjon et al., 2008), whereas values used for different variants of ENLM have been obtained as discussed in Section III (B).

A. Experiment I: Performance Analysis of the Proposed Algorithm. In this section, we have applied the proposed ENLM algorithm to noisy T1-w and T2-w simulated brain MRI. The performance of the proposed ENLM algorithm has been compared with UNLM at different noise levels. Figure 5 quantitatively compares the performance of UNLM and the proposed ENLM algorithm in terms of PSNR for T1-w and T2-w simulated brain MRI. As shown in Figure 5, the proposed ENLM algorithm outperforms UNLM at all noise levels. The advantage of ENLM is more prominent in case of T2-w brain MRI, where the performance boost of ENLM is more compared with T1-w brain MRI.

The denoising results using UNLM and the proposed ENLM algorithm have also been compared qualitatively. Figure 6 shows T1-w and T2-w brain images corresponding to a particular slice from the 3D simulated brain volume. Rician noise (10%) has been added to the said images prior to denoising using UNLM and the proposed ENLM algorithm. Third and fourth columns of Figure 6 present the images restored by using UNLM and the proposed ENLM algorithm. It can be observed visually that quality of the image restored by ENLM is better compared with UNLM-filtered image. The proposed ENLM algorithm better preserves minute image details (see the zoomed portions in Fig. 6). The contrast of the ENLM-filtered image is also better compared with UNLM-filtered image.

B. Experiment II: Influence of Optimization and Proposed SMF Process. In this section, we have investigated the influence of the proposed selective median filtering (SMF) and parameters optimization process on denoising performance. In particular, ENLM and $ENLM_s$ have been applied to T1-w and T2-w simulated brain MRI in order to compare the performance of the proposed algorithm with and without the application of proposed SMF process, respectively. Similarly, the comparison of $ENLM_o$ and ENLM helps realizing the performance advantage caused by the optimization of ENLM which was performed in Section III (B). Figure 7 compares the performance of the three variants of ENLM on simulated T1-w and T2-w brain MRI. The results have been presented in terms of both PSNR and SSIM. By comparing the performance of $ENLM_o$ and ENLM, it can be concluded that the process of optimization improves denoising performance for both T1-w and

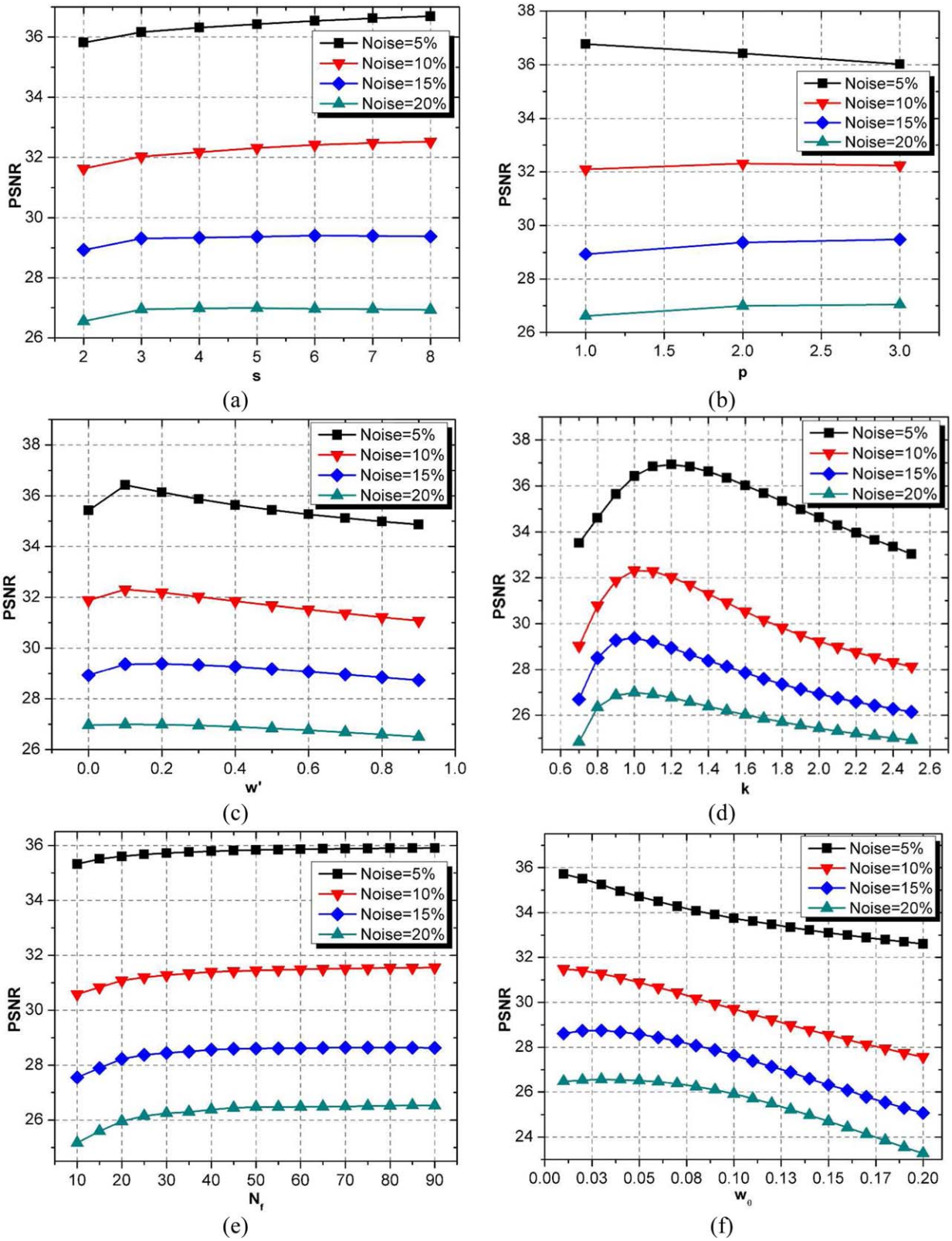

Figure 4. Optimal selection of (a) Search window size (*s*), (b) Patch size (*p*), (c) Central pixel weight (*w'*), (d) Scaling factor (*k*), (e) Number of fit patches (N_f), and (f) Weight threshold (w_θ). [Color figure can be viewed in the online issue, which is available at wileyonlinelibrary.com.]

T2-w brain MRI. Similarly, the inclusion of proposed SMF process significantly improves denoising results, especially at higher noise levels (see $ENLM_s$ and ENLM).

C. Experiment III: Comparison with Other Contemporary Methods. In Section IV (A), we compared the performance of the proposed ENLM algorithm with Unbiased NLM (UNLM)

Table I. Parameters' values used for different denoising algorithms.

	Parameters							
	w	p	k	N_f	w_θ	w'	Wavelet	$\sigma_{spatial}$
UNLM	5	2	1.2	–	–	Max	–	–
$ENLM_o$	5	2	1.2	27	0.01	Max	–	–
ENLM	5	2	1	60	0.01	0.1	–	–
OWT SURE-LET	–	–	–	–	–	–	sym8	–
Bayes	3	–	–	–	–	–	–	0.5

algorithm. In this section, we have compared the performance of the proposed ENLM algorithm, on T1-w simulated brain MRI denoising, with two other state of the art denoising methods. The first method is based on an approach of conditional posterior sampling which aims to find a general Bayes estimate of the noise-free image in the least-square sense (Wong et al., 2010). The second method is a wavelet-domain method that minimizes the mean square error between the noise-free and restored images (Luisier et al., 2007). The mean square error is estimated from an unbiased risk estimate called SURE (Stein's Unbiased Risk Estimate). Figure 8 shows the results, in terms of PSNR, for various denoising methods compared in this section. Clear advantage of the proposed algorithm is immediately

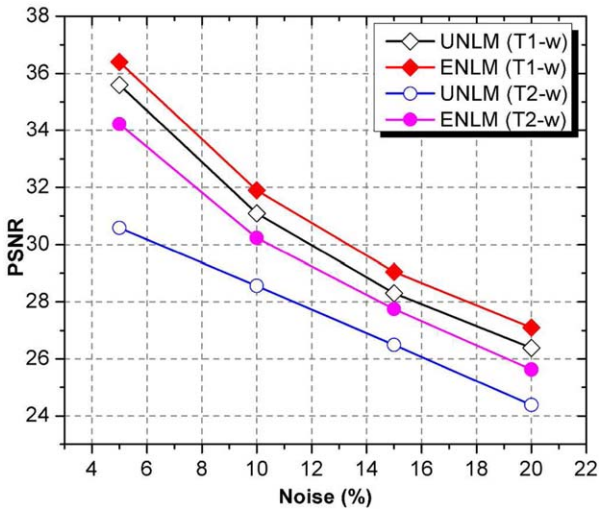

Figure 5. Performance comparison (in terms of PSNR) of UNLM and the proposed ENLM algorithm. [Color figure can be viewed in the online issue, which is available at wileyonlinelibrary.com.]

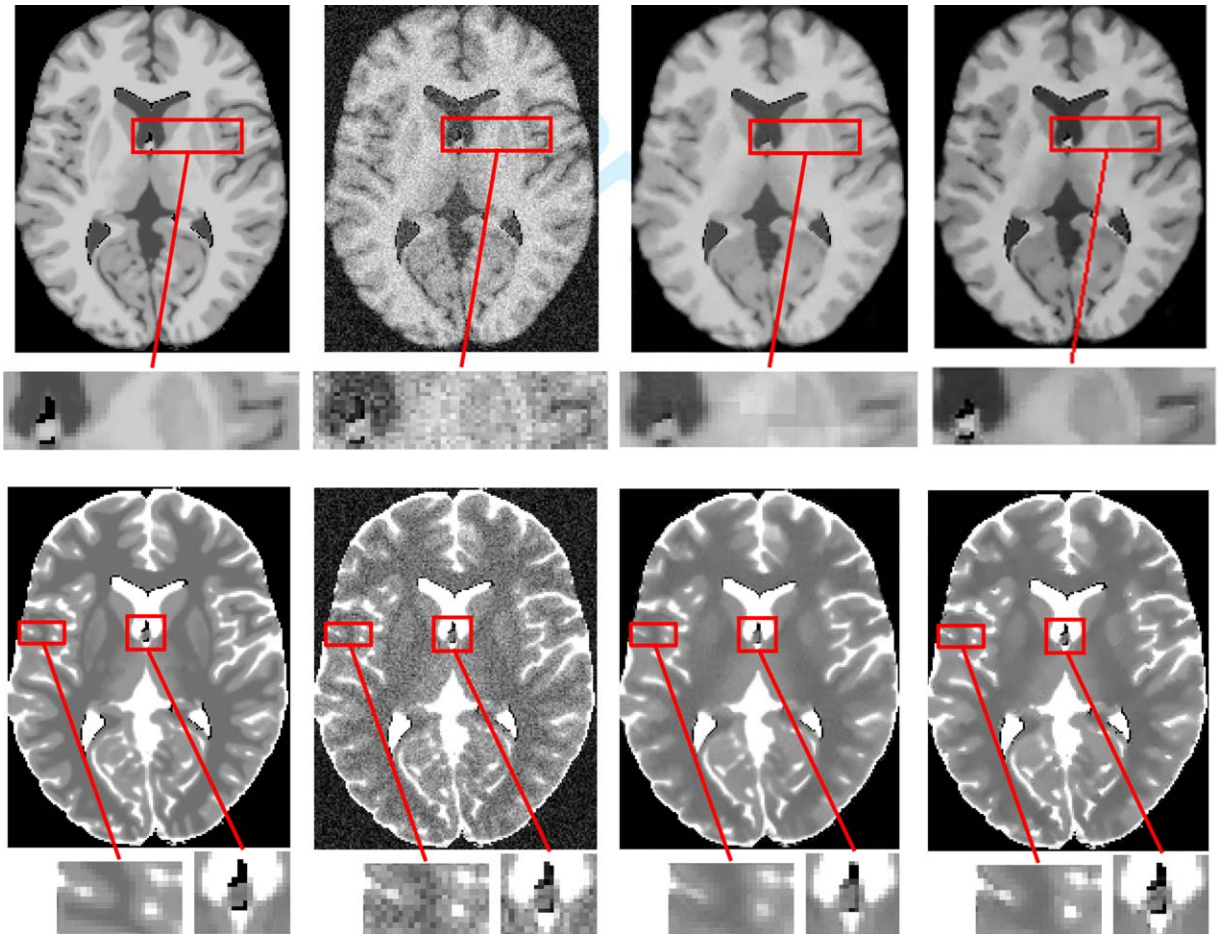

Figure 6. Performance comparison (visual) of the proposed ENLM algorithm with UNLM. First row: T1-w brain images. Second row: T2-w brain images. First and second column: original and noisy (noise = 10%) images, respectively. Third and fourth column: images filtered by UNLM and ENLM, respectively. [Color figure can be viewed in the online issue, which is available at wileyonlinelibrary.com.]

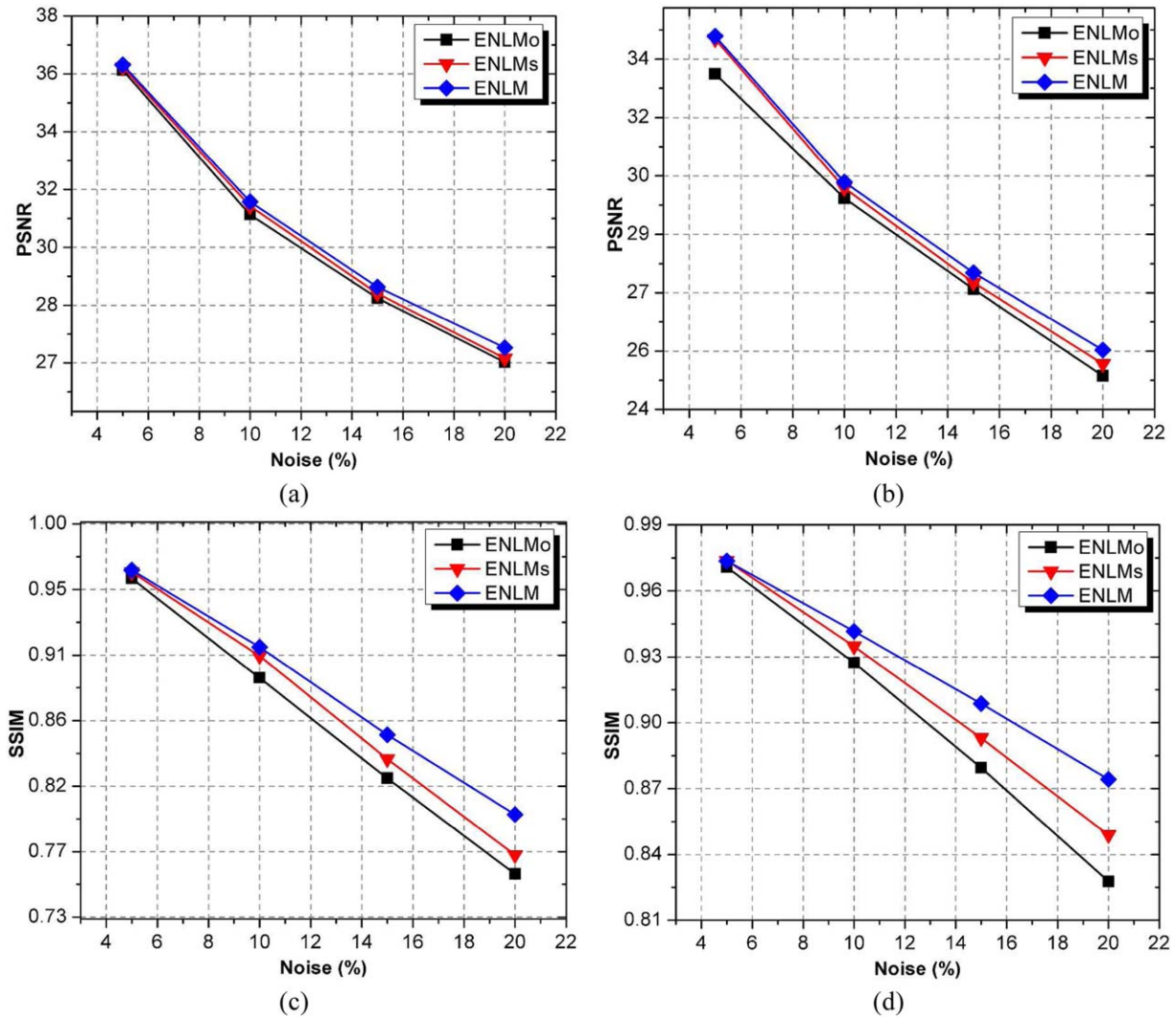

Figure 7. Impact of SMF and parameter optimization process on denoising performance of ENLM. [Color figure can be viewed in the online issue, which is available at wileyonlinelibrary.com.]

visible compared with other methods. The images restored using different methods have also been compared visually in Figure 9, for an input image corrupted with 10% Rician noise. The proposed ENLM method restores a cleaner image, while other methods produce much blurred images with noise artifacts still present in the images. Hence, the proposed ENLM algorithm supersedes other methods both quantitatively and qualitatively.

D. Experiment IV: Performance Comparison on T2-Weighted Brain MRI with MS Lesion. Medical images usually contain small structures which encapsulate pathologically important information. An effective denoising method should preserve such structures during the restoration process. In this section, we have applied the proposed ENLM method to denoise a T2-weighted brain MR image with multiple sclerosis (MS) lesion. Rician noise (10%) has been added to the said image (see Fig. 10) and denoising result of the proposed algorithm has been visually compared with UNLM. Figures 10c and 10d show the filtered images using UNLM and ENLM, respectively. It can be observed by visual inspection of the highlighted area in Figure 10 that the proposed ENLM algorithm better preserves the MS lesion structures. Therefore, the proposed ENLM algorithm is much suitable for medical applications which extract useful information from the MS lesion structures.

V. EXPERIMENTS ON REAL BRAIN MRI

Clinical MR images are usually corrupted with Ricain noise of unknown intensity. Therefore, a suitable method is inevitable for estimating the amount of noise present in real MRI data. Several methods have been proposed in literature to attack the said problem (Sijbers et al., 1998; Nowak, 1999; Fernandez et al., 2008). We have estimated the noise from real brain MRI using background part of the square magnitude MR images (Fernandez et al., 2008). The noise estimation method has already been described in Section II (A).

We have denoised real brain MRI (see Section III (A)) using the proposed ENLM algorithm and compared its performance qualitatively with UNLM. Figure 11 shows T1-w and T2-w noisy brain MR images from OASIS database and corresponding restored images using ENLM and UNLM. In order to compare the two images more diligently, selected portions of the noisy and restored images are also shown in zoomed view. It can be seen from Figure 11 that, similar to

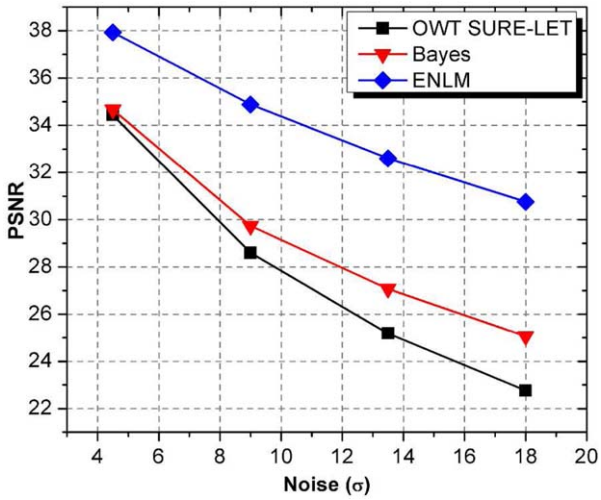

Figure 8. Performance comparison of the proposed ENLM algorithm on T1-w brain MRI with two contemporary methods. [Color figure can be viewed in the online issue, which is available at wileyonlinelibrary.com.]

simulated MRI denoising, the proposed ENLM algorithm better preserves small structures in the restored images compared with UNLM.

VI. APPLICATION TO BRAIN MRI SEGMENTATION

In many practical medical systems, segmentation is a successive step after denoising. Accurate segmentation depends critically on effective denoising. An effective denoising method preserves original structures in the restored image which, in turn, leads to better segmentation. On the other hand, a poor denoising may introduce undesirable artifacts in the restored image, thereby resulting in deteriorated segmentation. Successively, the quality of segmentation affects the classification of medical images (Chaudhry et al., 2013). Therefore, in this section, we have investigated the impact of the proposed ENLM algorithm on segmentation of simulated brain MRI. Generally, four major segments are present in a brain MR image: three types of brain tissues and a background segment. The three brain tissue types are gray matter (GM), white matter (WM) and cerebrospinal fluid (CSF) which should be accurately demarcated by the segmentation algorithm. However, Brain MRI suffers from a very common problem of Partial volume effect (PVE). PVE refers to the fact that in a particular voxel of a brain MRI volume, several types of tissues may overlap with each other. Therefore, characterizing each voxel discretely as part of a particular tissue type is not a suitable approach. In this regard, fuzzy segmentation techniques, which intrinsically deal with the PVE problem, prove to be quite successful. These techniques output a fuzzy membership matrix which describes the membership of each voxel to each tissue type. Thus, the tissue overlap problem is inherently dealt with the help of fuzzy membership values.

Fuzzy c-means (FCM) is an unsupervised segmentation technique based on iterative update of fuzzy membership values (Bezdek et al., 1984). Several variants of classical FCM have been proposed in literature (Chuang et al., 2006; Cai et al., 2007; Krinidis and Chatzis, 2010; Hassan et al., 2012). Fuzzy c-means with non-local spatial information (FCM_NLS) is a variant of FCM which modifies the

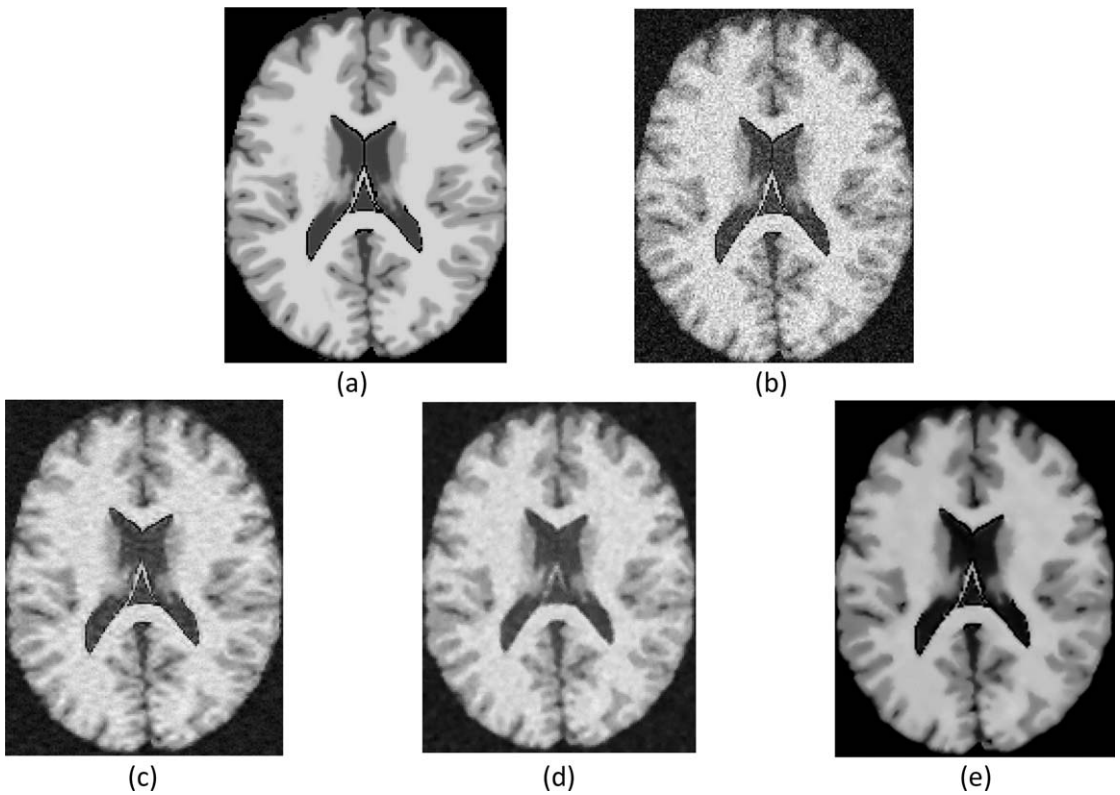

Figure 9. Performance comparison (visual) of the proposed ENLM algorithm with two contemporary methods. (a, b) T1-w original and noisy brain images, respectively. Image restored by (c) OWT SURE-LET method, (d) Bayesian estimation denoising method, and (e) the proposed ENLM algorithm.

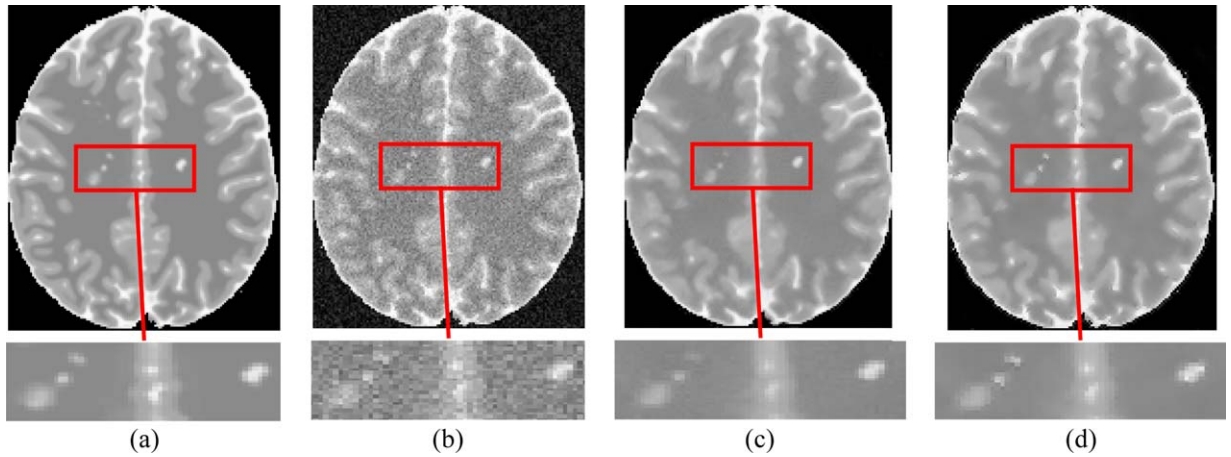

Figure 10. Performance of the proposed ENLM algorithm on T2-w brian MRI with MS lesion, (a) Original T2-w image, (b) Noisy image (noise = 10%), (c) UNLM-filtered image, (d) ENLM-filtered image. [Color figure can be viewed in the online issue, which is available at wileyonlinelibrary.com.]

objective function of classical FCM by incorporating non-local spatial information (Zhao et al., 2011). The non-local information is integrated into the segmentation framework by adding a non-local term into the objective function of classical FCM. The non-local term is computed from the image restored by NLM instead of the original image. Thus, FCM_NLS minimizes an objective function which is computed from both the original and NLM-restored image. In this section, we have tested the impact of the proposed ENLM algorithm on segmentation performance by computing the non-local term of FCM_NLS using ENLM-restored image instead of NLM-restored image. The resulting segmentation algorithm is named as Fuzzy c-means with enhanced non-local information (FCM_ENL) in the following text. The objective function of FCM_ENL (see Zhao et al., 2011) is given as follows.

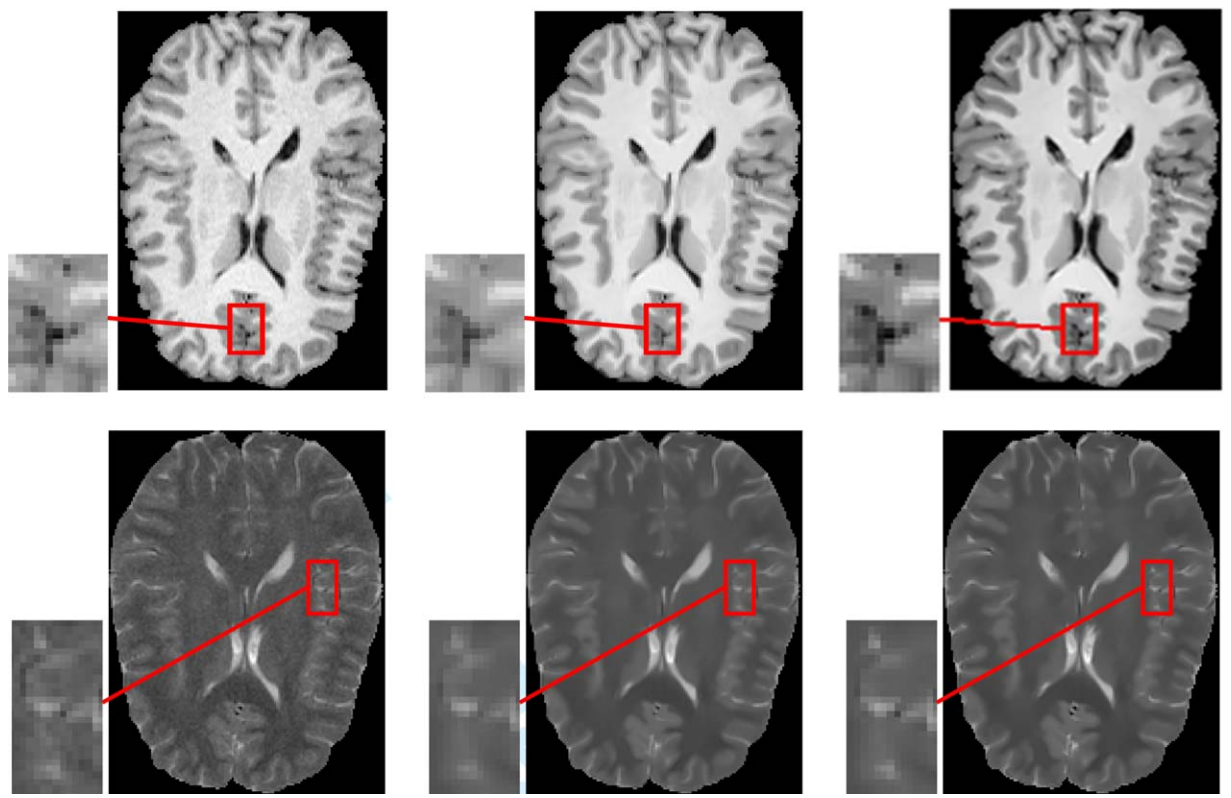

Figure 11. Performance comparison (visual) of the proposed ENLM algorithm with UNLM on real brain MRI. First row: T1-w real brain images. Second row: T2-w real brain images. First column: original images. Second and third column: images filtered by UNLM and ENLM, respectively. [Color figure can be viewed in the online issue, which is available at wileyonlinelibrary.com.]

Table II. Performance comparison (in terms of SA and RI) of different segmentation techniques.

		Segmentation Technique				
	Noise (%)	SFCM	FGFCM	FLICM	FCM_UNL	FCM_ENL
SA	5	0.9534	0.9516	0.9454	0.9592	0.9617
	9	0.9027	0.9117	0.9277	0.9305	0.9351
	13	0.7951	0.8371	0.8589	0.8961	0.9052
	15	0.7197	0.7662	0.7980	0.8779	0.8906
RI	5	0.8794	0.8762	0.8654	0.8949	0.9003
	9	0.7649	0.7868	0.8266	0.8280	0.8382
	13	0.5739	0.6538	0.7162	0.7544	0.7736
	15	0.4803	0.5582	0.6397	0.7181	0.7434

$$J_m = \sum_{k=1}^{c}\sum_{i=1}^{n} u_{ki}^{m}\|y_i - v_k\|^2 + \beta \sum_{k=1}^{c}\sum_{i=1}^{n} u_{ki}^{m}\|x_i' - v_k\|^2 \quad (8)$$

where, y_i and x_i' are intensity values of ith noisy pixel and corresponding ENLM-restored pixel, respectively. v_k designates the kth cluster centroid, whereas u_{ki} represents fuzzy membership of pixel i to cluster k. Number of clusters and number of input image pixels are denoted by c and n, respectively. The second term in Eq. (8) takes into account the non-local information. The parameter β controls the tradeoff between the amount of information exploited from input and restored images.

We have compared the performance of the proposed algorithm based FCM_ENL with a few other segmentation techniques on simulated brain MRI segmentation. These techniques include spatial fuzzy c-means (SFCM) (Chuang et al., 2006), fast generalized fuzzy c-means (FGFCM) (Cai et al., 2007), fuzzy local information c-means (FLICM) (Krinidis and Chatzis, 2010) and fuzzy c-means with unbiased non-local information (FCM_UNL) (Zhao et al., 2011). FCM_UNL is similar to FCM_ENL, however, it employs UNLM-restored image in the non-local term of its objective function instead of ENLM-restored image. The segmentation results are reported for each technique in terms of segmentation accuracy (SA), Rand index (RI), and dice coefficient (DC). SA (the ratio of number of correctly labeled pixels to total number of pixels) and RI (Rand, 1971) are quantitative measures to assess the overall accuracy of a

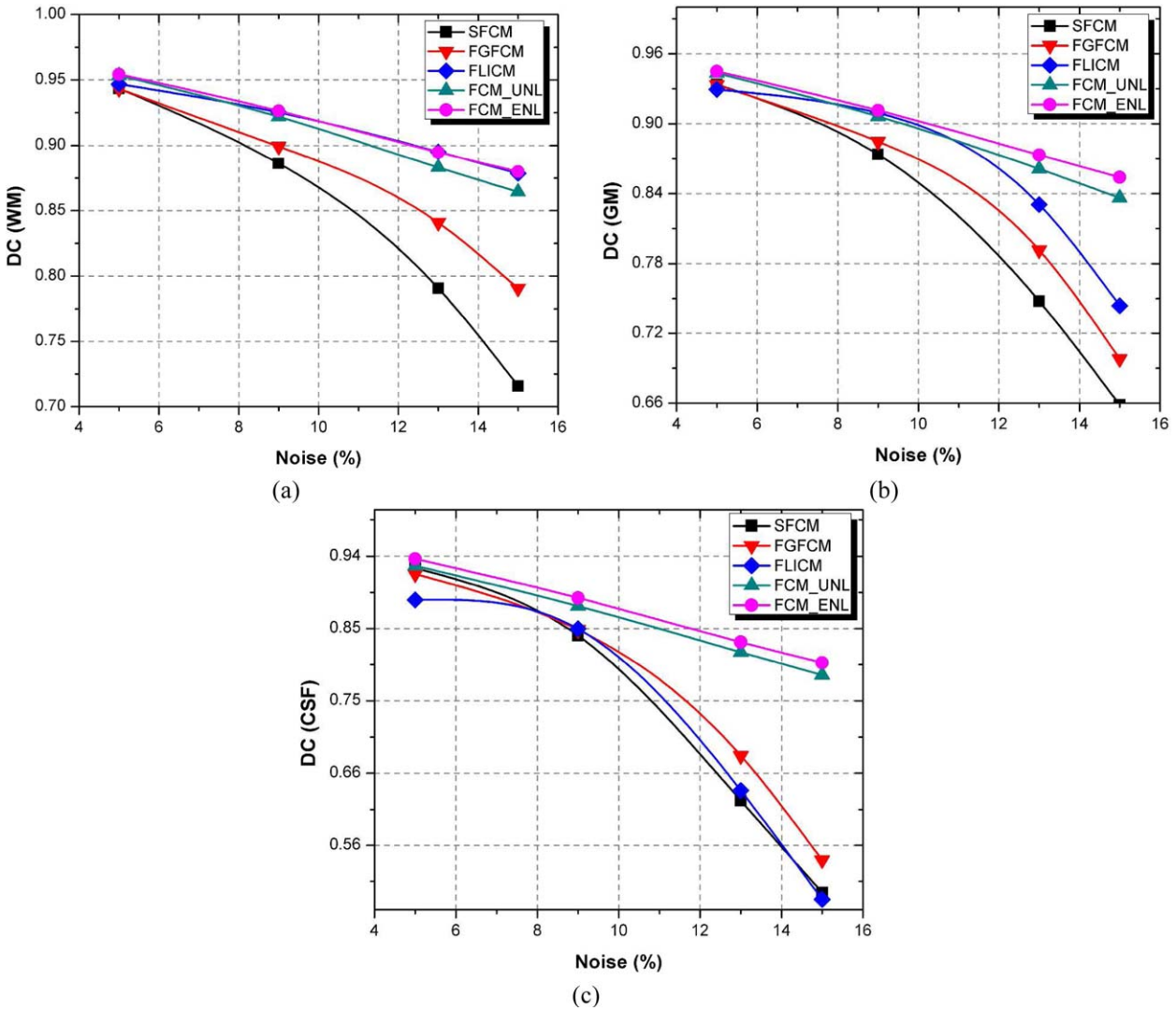

Figure 12. Performance comparison (in terms of DC) of the proposed ENLM based FCM_ENL segmentation with other techniques for, (a) WM, (b) GM, (c) CSF. [Color figure can be viewed in the online issue, which is available at wileyonlinelibrary.com.]

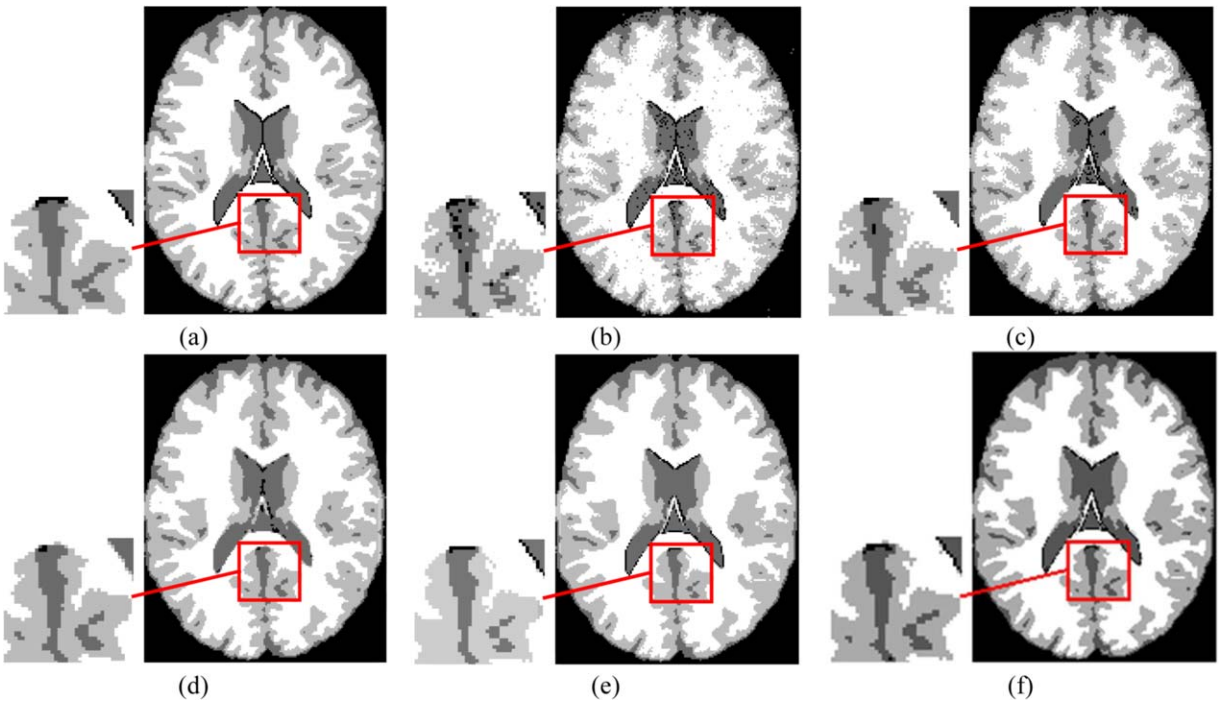

Figure 13. Performance comparison (visual) of different segmentation techniques. (a) Ground truth image with four segments, image segmented by (b) SFCM, (c) FLICM, (d) FGFCM, (e) FCM_UNL, (f) Proposed ENLM algorithm based FCM_ENL. [Color figure can be viewed in the online issue, which is available at wileyonlinelibrary.com.]

segmentation technique. RI is computed using the following mathematical expression.

$$\mathrm{RI} = \frac{a+b}{a+b+c+d} \tag{9}$$

where a, b, c, and d represent number of different pairs of elements in the ground truth (G) and segmented (S) images. In particular, a represents the number of pairs assigned to same clusters in S and in G, and d represent number of pairs assigned to the different clusters in S and in G. On the other hand, b represents number of pairs assigned to different clusters in S and same clusters in G, and c represents number of pairs assigned to same clusters in S and different clusters in G.

Dice coefficient (DC) is used to measure the effectiveness of delineating each segment separately. DC has been employed for assessing the segmentation accuracy as segregating each tissue separately in brain MRI is important in certain medical applications. For each segment, the dice coefficient is computed using the following expression.

$$\mathrm{DC}\,(S_i, G_i) = \frac{2|S_i \cap G_i|}{|S_i| + |G_i|}, \qquad \forall\ i \in c \tag{10}$$

where, G_i and S_i represent the set of pixels in the ith segment of ground truth and segmented images, respectively. Legal values of SA, RI and DC range from 0 to 1.

A. Quantitative Comparison. Table II compares SA and RI values for each technique, applied to simulated brain MRI at different noise levels. It can be observed from the quantitative measures in Table II that the proposed ENLM algorithm based FCM_ENL technique outperforms all other algorithms at all noise levels. The results are consistent for both the evaluation measures. The performance advantage of FCM_ENL becomes even more evident with increasing noise levels. Therefore, it can be reasonably concluded that FCM_ENL is robust to noise compared with other techniques.

Figure 12 shows a graphical comparison of different segmentation techniques in terms of DC values. Figures 12a to 12c correspond to WM, GM, and CSF segments, respectively. It can be concluded by comparing results in Figure 12 that FCM_ENL performs superior segmentation of each tissue compared with other segmentation techniques. Particularly, in case of CSF, FCM_ENL yields significantly improved segmentation compared with other techniques. Hence, FCM_ENL not only provides overall best accuracy, but also better handles segmentation of individual tissue types.

B. Qualitative Comparison. Finally, we have compared visual segmentation results, produced by the proposed ENLM algorithm based FCM_ENL and other segmentation techniques used in this work. The ground truth of segmentation is available for simulated brain MRI data set which we have used in our comparison. Therefore, visual segmentation results, produced by different techniques, can be easily validated against the ground truth segmentation. Figure 13a shows the ground truth segmentation for a brain image from the Brainweb simulated brain MRI data set. Figures 13b to 13f show corresponding segmentation results produced by different segmentation techniques at 10% noise. For a more convenient comparison, a selected portion of each image is displayed in zoomed view. It can be concluded by visual inspection of the images that the proposed ENLM based FCM_ENL produces a segmentation that bears maximal similarity with the ground truth. The images segmented by other techniques contain misclassified pixels due to under- or over-segmentation. Therefore, it can be concluded reasonably that the proposed ENLM algorithm boosts the performance of segmentation process.

VII. CONCLUSION

Brain MR Images are corrupted by Rician noise, which should be removed with an effective denoising method in order to obtain reasonable results in subsequent treatment of these images. NLM is a popular denoising method based on weighted averaging of image pixels within a non-local window. IANLM is a variant of classical NLM which proposes making the window size adaptive based on a robust threshold criterion. In this work, we have proposed an enhanced non-local means (ENLM) algorithm for application to brain MRI by introducing certain extensions to IANLM. First, in ENLM, the IANLM algorithm has been adapted to Rician noise in magnetic resonance images by applying a Rician bias correction procedure. Second, a selective median filtering procedure has been proposed as a post processing step in order to overcome limitations of IANLM. Third, different parameters of the proposed ENLM algorithm have been optimized for application to brain MRI. In order to investigate the influence of the modifications proposed in ENLM, different variants of the proposed ENLM algorithm have been validated on both T1-w and T2-w simulated and real brain MRI. Improved quantitative and qualitative results have been obtained by ENLM compared with other denoising algorithms. Additionally, the proposed algorithm has been applied to a T2-w brain MR image with MS lesion in order to show that the algorithm effectively preserves pathologically important information. Finally, the impact of the proposed ENLM algorithm on segmentation has also been investigated, and improved segmentation results (both quantitative and qualitative) have been obtained compared with other state of the art segmentation techniques.

ACKNOWLEDGMENTS

The authors express their appreciation for McConnell Brain Imaging Center (BIC) of the Montreal Neurological Institute, for publicly sharing the simulated brain MR data (BrainWeb, http://www.bic.mni.mcgill.ca/brain-web). The authors also acknowledge Randy Buckner, Daniel Marcus, and Washington University Alzheimer's Disease Research Center for sharing Open Access Series of Imaging Studies (OASIS, www.oasis-brains.org) real brain MRI database. Finally, the authors are highly obliged to David Fernandez-Prim for providing the MATLAB on-figure magnifier tool (http://www.mathworks.com/matlabcentral/fileexchange/26007-on-figure-magnifier), which greatly simplified the task of presentation of figures used in this work.

REFERENCES

A. Buades, B. Coll, and J.M. Morel, A review of image denoising algorithms with a new one, Multiscale Model Simul, 4 (2005), 490–530.

A. Chaudhry, M. Hassan, A. Khan, J. Kim, Automatic active contour-based segmentation and classification of carotid artery ultrasound images, J Digital Imaging 26 (2013), 1071–1081.

A. Macovski, Noise in MRI, Magn Reson Med, 36 (1996), 494–497.

A. Wong, A. Mishra, K. Bizheva, and D.A. Clausi, General Bayesian estimation for speckle noise reduction in optical coherence tomography retinal imagery, Optics Express 18 (2010), 8338–8352.

A.T. Vega, V.G. Perez, S.A. Fernandez, and C.F. Westin, Efficient and robust non-local means denoising of MR data based on salient features matching, Comput Methods Programs Biomed 105 (2012), 131–144.

C. Tomasi and R. Manduchi, "Bilateral filtering for gray and color images," In Sixth International Conference on Computer Vision, Bombay, 1998, pp. 839–846.

D. Donoho, De-noising by soft-thresholding, IEEE Trans Inform Theor, 41 (1995), 613–627.

D.L. Collins, A.P. Zijdenbos, V. Kollokian, J.G. Sled, N.J. Kabani, C.J. Holmes, and A.C. Evans, Design and construction of a realistic digital brain phantom, IEEE Trans Med Imaging, 17 (1998), 463–46.

D.S. Marcus, T.H. Wang, J. Parker, J.G. Csernansky, J.C. Morris, and R.L. Buckner, Open Access Series of Imaging Studies (OASIS): Cross-sectional MRI data in young, middle aged, nondemented, and demented older adults, J Cogn Neurosci, 19 (2007), 1498–1507.

F. Luisier, T. Blu, and M. Unser, A new SURE approach to image denoising: Interscale orthonormal wavelet thresholding, IEEE Trans Image Process, 16 (2007), 593–606.

F. Zhao, L. Jiao, and H. Liu, Fuzzy c-means clustering with non local spatial information for noisy image segmentation, Front Comput Sci China 5 (2011), 45–56.

I. Aksam, S. Rathore, and A. Jalil, Parameter optimization for non-local denoising using elite GA, In 15th International Multitopic Conference (INMIC), Islamabad, 2012, pp. 194–199.

J.C. Bezdek, R. Ehrlich, and W. Full, FCM: The Fuzzy C-Means clustering algorithm, Comput Geosci, 10, 191–203.

G. Gilboa, N. Sochen, and Y.Y. Zeevi, Image enhancement and denoising by complex diffusion processes, IEEE Trans Pattern Anal Machine Intell, 26 (2004), 1020–1036.

H. Gudbjartsson and S. Patz, The rician distribution of noisy MRI data, Magn Reson Med, 34 (1995), 910–914.

I.M. Aksam, A. Jalil, S. Rathore, A. Ali, and M. Hussain, Brain MRI denoizing and segmentation based improved adaptive non-local means, Int J Imaging Syst Technol, 23 (2013), 235–248.

I.W. Selesnick, The double-density dual-tree DWT, IEEE Trans Signal Process, 52 (2004), 1304–1314.

J. Salmon, On two parameters for denoising with non-local means, Signal Process Lett, 17 (2010), 269–272.

J. Sijbers, A.J.D. Dekker, D.V. Dyck, and E. Raman, Estimation of signal and noise from Rician distributed data, Proc Int Conf Signal Process Commun, 1998, 140–142.

J.V. Manjon, J.C. Caballero, J.J. Lull, G.G. Marti, L.M. Bonmati, and M. Robles, MRI denoising using non-local means, Med Image Anal, 12 (2008), 514–523.

J.V. Manjon, P. Coupe, L.M. Bonmatí, D.L. Collins, and M. Robles, Adaptive non-local means denoising of MR images with spatially varying noise levels, J Magen Reson Imaging, 31 (2010), 192–203.

K.S. Chuang, H.L. Tzeng, S. Chen, J. Wu, and T.J. Chen, Fuzzy c-means clustering with spatial information for image segmentation, Comput Med Imaging Graph, 30 (2006), 9–15.

L.P. Yaroslavsky, Digital Picture Processing. An Introduction. Springer-Verlag, Berlin (1985), ISBN 3-540-11934-5.

M. Hassan, A. Chaudhry, A. Khan, J. Kim, T. Tuan, Carotid artery image segmentation using modified spatial fuzzy c-means and ensemble clustering, Comput Methods Programs Biomed 108 (2012), 1261–1276.

MATLAB, MATLAB—The Language of Technical Computing, The MathWorks, Inc., Natick, Massachusetts, 2013.

MIPAV, Medical Image Processing, Analysis and Visualization, Imaging Sciences Laboratory, Center for Information Technology, Bethesda, MD, 2013.

OriginPro, Data Analysis and Graphing Software, OriginLab Corporation, Northampton, 2012.

P. Perona and J. Malik, Scale-space and edge detection using anisotropic diffusion, IEEE Trans Pattern Anal Mach Intell, 12 (1990), 629–639.

R. Yan, L. Shao, S.D. Cvetkovic, and J. Klijn, Improved non-local means based on pre-classification and invariant block matching, J Display Technol 8 (2012), 212–218.

R.D. Nowak, Wavelet-based Rician noise removal for magnetic resonance imaging, IEEE Trans Image Process, 8 (1999), 1408–1419.

R.K.S. Kwan, A.C. Evans, and G.B. Pike, An extensible MRI simulator for post-processing evaluation, visualization in biomedical computing, Lecture notes in computer science, Springer-Verlag, Berlin, 1996, pp. 135–140.

S. Grewenig, S. Zimmer, and J. Weickert, Rotationally invariant similarity measures for non-local image denoising, J Vis Commun Image Represent, 22 (2011), 117–130.

S. Krinidis and V. Chatzis, A robust fuzzy local information C-means clustering algorithm, IEEE Trans Image Process, 19 (2010), 1328–1337.

S. Osher, M. Burger, D. Goldfarb, J. Xu, and W. Yin, An iterative regularization method for total variation-based image restoration, Multiscale Model Simul, 4 (2005), 460–489.

S.A. Fernandez, C.A. Lopez, and C.F. Westin, Noise and signal estimation in magnitude MRI and Rician distributed images: A LMMSE approach, IEEE Trans Image Process, 17 (2008), 1383–1398.

T. Thaipanich and C.C.J. Kuo, An adaptive non-local means scheme for medical image denoising, Proc. SPIE 7623 Medical Imaging, California, 2010.

W. Cai, S. Chen, and D. Zhang, Fast and robust fuzzy c-means clustering algorithms incorporating local information for image segmentation, Pattern Recognit, 40 (2007), 825–838.

W.M. Rand, Objective criteria for the evaluation of clustering methods, J Am Stat Assoc, 66 (1971), 846–850.

Wiest-Daesslé, S. Prima, P. Coupé, S.P. Morrissey, and C. Barillot, Rician noise removal by non-Local Means filtering for low signal-to-noise ratio MRI: Applications to DT-MRI, MICCAI, 2008, 171–179.

Y.L. Liu, J. Wang, X. Chen, Y.W. Guo, and Q.S. Peng, A robust and fast non-local means algorithm for image denoising, J Comput Sci Technol, 23 (2008), 270–279.

Z. Wang, A.C. Bovik, H.R. Sheikh, and E.P. Simoncelli, Image quality assessment: from error visibility to structural similarity, IEEE Trans Image Process, 13 (2004), 600–612.